Spatial morphology of macroscopic superposition of three-dimensional coherent laser waves in degenerate cavities

T. H. Lu, Y. F. Chen,* and K. F. Huang
Department of Electrophysics, National Chiao Tung University, Hsinchu, Taiwan
(Received 12 November 2007; published 25 January 2008)

We employ high-order degenerate laser cavities to analogously investigate the morphology of macroscopic superposition states of three-dimensional coherent waves. The spatial features of macroscopic superposition states are found to exhibit dashed and dotted wave patterns. We evaluate the mode volume to explore the domination of macroscopic superposition states. A large-aperture laser resonator is experimentally implemented to confirm the theoretical results.

DOI: 10.1103/PhysRevA.77.013828 PACS number(s): 42.25.Ja, 42.60.Jf, 03.65.−w

I. INTRODUCTION

The coherent superposition principle has attracted a great deal of attention because it plays a significant role in exploring the boundary between microscopic and macroscopic worlds [1–3]. The macroscopic superposition states, generally referred to as Schrödinger cat states [4], illustrate a remarkable contrast between the quantum world and the classical experience. So far, some progress has been made in demonstrating the macroscopic superposition states in various systems such as the Rydberg atomic electron states [5], photons in a microwave cavity [6], and the superconducting condensate [7]. Despite that, there has been no experimental demonstration of the morphologies of wave functions concerning the macroscopic superposition states.

In the past few decades, the quantum formulism has been increasingly recognized to be of great importance in describing distinct branches of physics because of the underlying structural similarity. For instance, the quantum description has been applied to numerous areas, including charged-particle-beam physics [8], plasma physics [9], nonlinear optics [10], mesoscopic physics [11], and laser physics [12–15]. One of the most striking and profound similarities is that the electromagnetic wave equation in paraxial approximation is isomorphous to the Schrödinger equation [16]. This analogy has been increasingly used to provide an experimental visualization in optical context for confirming many quantum effects, such as quantum chaos phenomena [17,18], disorder-induced wave localization [19], geometric phases [20], and the issue of quantum tunneling [21].

Spatial structures of laser modes in broad-area resonators have recently received much interest for providing a deep insight into the pattern formation of natural waves [22–30]. More recently, the three-dimensional (3D) coherent laser modes emitted from degenerate cavities have been precisely explained via the quantum stationary coherent states of the commensurate anisotropic 2D harmonic oscillator [31–36]. The excellent conformity between the experimental laser waves and the quantum coherent states enables us to utilize the laser coherent waves to look into the spatial morphology of macroscopic coherent superposition.

In this work we present analogous investigations on the spatial morphology of macroscopic coherent superposition with the 3D coherent laser waves that have been experimentally confirmed to be generic stationary modes in large-Fresnel-number degenerate resonators. We start by numerically demonstrating that the superposition of two 3D coherent waves brings about the emergence of spatially discrete localized patterns that include various dashed and dotted wave patterns. To realize the macroscopic superposition states, we make use of a high-quality degenerate laser cavity to excite extremely high-order coherent stationary modes. Experimental observations not only confirm the existence of the superposition of 3D coherent laser waves, but also provide striking information for the morphologies of macroscopic quantum superposition states in an analogous way.

II. MORPHOLOGY OF THE MACROSCOPIC SUPERPOSITION OF 3D COHERENT WAVES

Experimental observations manifested that the longitudinal-transverse coupling and the mode-locking effect in large-Fresnel-number spherical laser cavities generally drive the bare ratio between the transverse and longitudinal mode spacing, Ω, to be locked to a rational number P/Q, forming an interesting fractal structure [36]. Consequently, the laser modes more often than not exhibit 3D coherent waves that are transversely localized on the Lissajous figures with the relative phase continuously varying with the longitudinal direction. Here we perform systematic numerical calculations for exploring the pattern formation of the superposition of 3D coherent waves. In terms of the quantum coherent state, the 3D coherent optical waves can be generally expressed as [36]

$$\psi^{p,q,s}_{m_o,n_o,l_o}(x,y,z)=\frac{1}{\sqrt{M+1}}\sum_{k=0}^{M}e^{ik\phi_o}\Phi^{(HG)}_{m_o+pk,n_o+qk,l_o+sk}(x,y,z), \tag{1}$$

where the parameter ϕ_o is the relative phase between the adjoining Hermite-Gaussian (HG) modes $\Phi^{(HG)}_{m,n,l}(x,y,z)$ which are given by [37]

*Corresponding author. FAX: (886) 35-725230. yfchen@cc.nctu.edu.tw

 ©2008 The American Physical Society

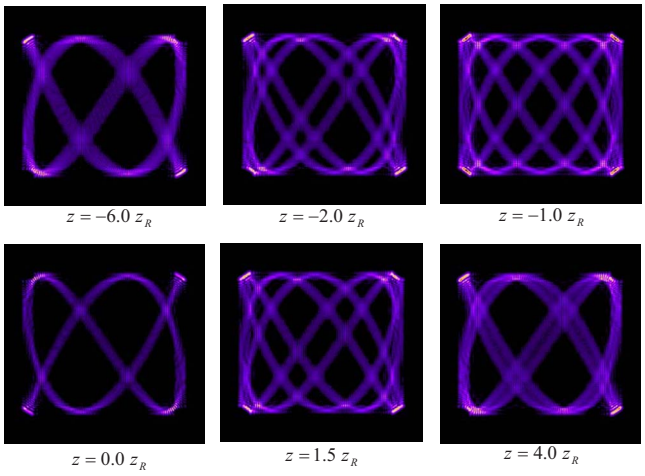

FIG. 1. (Color online) Numerical results for the tomographic transverse patterns of the 3D coherent state $\psi^{p,q}_{m_o,n_o}(x,y,z)$ described in Eq. (1) with $(m_o,n_o)=(100,100)$, $(p,q)=(5,-3)$, $P/Q=1$, $\phi_o=0$, and $M=6$.

$$\Phi^{(HG)}_{m,n,l}(x,y,z)=\frac{1}{\sqrt{2^{m+n-1}\pi m\,!\,n!}}\frac{1}{w(z)}H_m\left(\frac{\sqrt{2}x}{w(z)}\right)H_n\left(\frac{\sqrt{2}y}{w(z)}\right)\times e^{[(-x^2+y^2)/w(z)^2]}e^{i(m+n+1)\tan^{-1}(z/z_R)}\times e^{-i(\pi z/L)[l+(m+n+1)P/Q][(x^2+y^2)/2(z^2+z_R^2)+1]}, \quad (2)$$

where m and n are the indices of x and y coordinates, $w(z)=w_o\sqrt{1+(z/z_R)^2}$, w_o is the beam radius at the waist, L is the effective cavity length, and z_R is the Rayleigh range. Note that the order indices m_o, n_o, and l_o are greater than the number index M by far and the integer s is taken to be negative for convenience. Hereafter we abbreviate $\psi^{p,q,s}_{m_o,n_o,l_o}(x,y,z)$ to be $\psi^{p,q}_{m_o,n_o}(x,y,z)$ because the indices l_o and s obey the equations $l_o+(m_o+n_o+1)(P/Q)=2\lambda/L$ and $s+(p+q)(P/Q)=0$, respectively, where λ is the lasing wavelength. Figure 1 illustrates numerical results for the tomographic transverse patterns of the 3D coherent state $\psi^{p,q}_{m_o,n_o}(x,y,z)$ described in Eq. (1) with $(m_o,n_o)=(100,100)$, $(p,q)=(5,-3)$, $P/Q=1$, $\phi_o=0$, and $M=6$. It can be clearly seen that the transverse patterns of the 3D coherent wave are localized on the *Lissajous* curves with their relative phases varying with the position z. With the result of the spatial feature of the stationary coherent states of the 2D quantum harmonic oscillator [32–35], we can deduce that the 3D coherent waves $\psi^{p,q}_{m_o,n_o}(x,y,z)$ have the intensity distribution concentrated on the parametric surface:

$$x(\vartheta,z)=\sqrt{m_o}w(z)\cos\left[q\vartheta-\frac{\phi(z)}{p}\right],$$
$$y(\vartheta,z)=\sqrt{n_o}w(z)\cos(p\vartheta), \quad (3)$$

where $0\le\vartheta\le 2\pi$, $-\infty\le z\le\infty$, and the z-dependent phase factor is given by

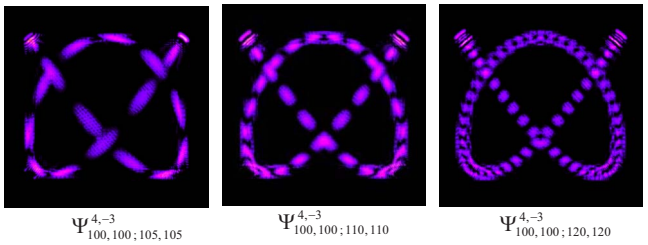

FIG. 2. (Color online) Numerical results for the transverse morphologies of three macroscopic superposition states $\Psi^{4,-3}_{100,100;105,105}$, $\Psi^{4,-3}_{100,100;110,110}$, and $\Psi^{4,-3}_{100,100;120,120}$ with $z=0$, $\phi_o=0$, and $M=6$.

$$\phi(z)=(q+p)\tan^{-1}(z/z_R)+\phi_o. \quad (4)$$

It is worth noting that the phase factor $\phi(z)$ of Eq. (4) arises from the Gouy-phase difference between the HG modes with distinct transverse orders.

In terms of the 3D coherent waves of Eq. (1), a superposition of two distinct coherent states can be generally written as

$$\Psi^{p,q}_{m_1,n_1;m_2,n_2}(x,y,z)=[\psi^{p,q}_{m_1,n_1}(x,y,z)+e^{i\phi}\psi^{p,q}_{m_2,n_2}(x,y,z)]/\sqrt{2}, \quad (5)$$

where ϕ is an arbitrary phase. The spatial feature of the macroscopic superposition of Eq. (5) can be manifested by setting $\phi=0$ without loss of generality. Figure 2 depicts numerical results for the transverse morphologies of three macroscopic superposition states $\Psi^{4,-3}_{100,100;105,105}$, $\Psi^{4,-3}_{100,100;110,110}$, and $\Psi^{4,-3}_{100,100;120,120}$ with $z=0$, $\phi_o=0$, and $M=6$. It can be seen that pair interference between 3D coherent waves gives rise to striking spatial features that consist of various dashed and dotted wave patterns. The distinction among the long-dashed, short-dashed, and dotted structures arises from the transverse-order difference $|n_1-n_2|$ and $|m_1-m_2|$ between two coherent states in $\Psi^{p,q}_{m_1,n_1;m_2,n_2}$. On the whole, increasing the transverse-order difference causes the spatial feature to change from a dashed wave pattern to a dotted wave pattern. To be brief, the macroscopic superposition of Eq. (5) reveals a striking phenomenon of the spatial beat that can be perceived as a spatially periodical variation in the 3D coherent waves. Although the transverse orders (m,n) of the numerical patterns in Figs. 1 and 2 are in the range of 100–140, the spatial features are nearly the same for the superposition of 3D coherent optical waves with higher transverse orders.

As shown in Fig. 1, the transverse pattern of the 3D coherent wave varies with the propagation position z because of the phase factor of Eq. (4). Therefore, the spatial feature of the macroscopic superposition is expected to reveal a similar revolution. Figure 3 depicts numerical results for the tomographic transverse patterns of the macroscopic superposition $\Psi^{3,-2}_{100,100;110,110}$ along the longitudinal z axis with $P/Q=1$, $\phi_o=\pi/2$, and $M=6$. It can be seen that the tomographic transverse patterns of the superposition of 3D coherent optical waves display the revolution of the spatially localized patterns along the longitudinal axis to form a complete 3D interference pattern. Similar spatial patterns can be extended to other waves of wave physics because of the analogy be-

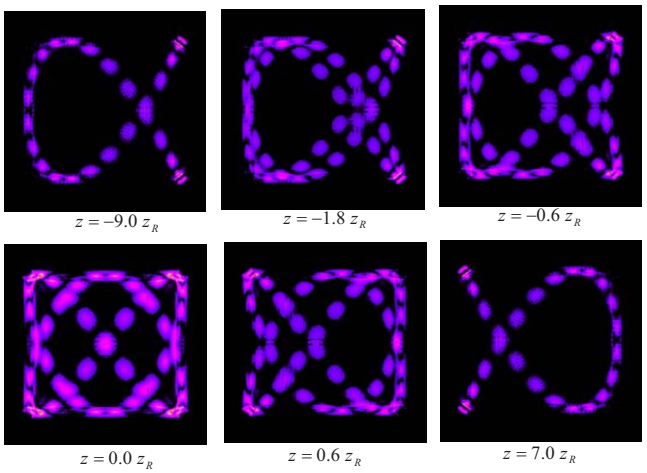

FIG. 3. (Color online) Numerical results for the tomographic transverse patterns of the macroscopic superposition $\Psi^{3,-2}_{100,100;110,110}$ along the longitudinal z axis with $P/Q=1$, $\phi_o=\pi/2$, and $M=6$.

tween the classical electromagnetic wave and other wave phenomena [8–15]. In particular, the paraxial wave equation for propagation along the z axis can be mapped onto the Schrödinger equation of a free particle in two dimensions, where the z coordinate is replaced by the time variable [16,38,39]. In the following, we will describe how to use a high-quality laser cavity to demonstrate the existence of these macroscopic superposition states.

III. REALIZATION OF MACROSCOPIC SUPERPOSITION STATES

To realize the macroscopic superposition states of 3D coherent laser waves, a critical issue that needs to be addressed is whether these states can be generated from large-Fresnel-number degenerate cavities. From the viewpoint of the stimulated emission, the coupling strength between the gain medium and the cavity mode is determined by the ratio Q/V_{eff}, where Q is the quality factor and V_{eff} is the effective mode volume. In general, there are numerous high-order cavity modes to have the Q factor close to the maximum value as long as these modes have optimal spatial overlaps with the pump distribution. Among these high-quality cavity modes, however, only the mode with the minimum mode volume can have the lowest lasing threshold to break into oscillation at first. For a normalized wave function Ψ, the mode volume is expressed as [40,41]

$$V_{eff} = \frac{1}{\int\int |\Psi|^4 dxdy}. \tag{6}$$

Figure 4 shows representative numerical results for the mode volume as a function of the transverse order m for the HG modes of Eq. (2), the 3D coherent waves of Eq. (1), and the macroscopic superposition of Eq. (5). The values of the parameters used in the calculation are as follows: $\phi=0$, $\phi_o=0$, $n=m$, $n_1=m_1=m$, $n_2=m_2=m+10$, $(p,q)=(3,-2)$, and $M=6$.

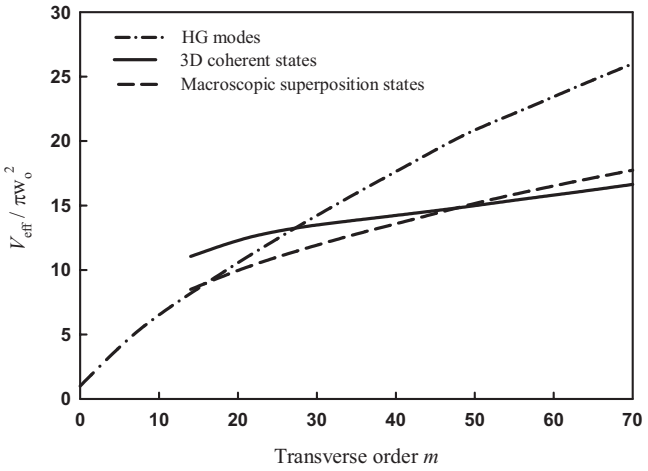

FIG. 4. Numerical results for the mode volume as a function of the transverse order m for the HG modes of Eq. (2), the 3D coherent waves of Eq. (1), and the macroscopic superposition of Eq. (5). The values of the parameters are as follows: $\phi=0$, $\phi_o=0$, $n=m$, $n_1=m_1=m$, $n_2=m_2=m+10$, $(p,q)=(3,-2)$, and $M=6$.

As seen in Fig. 4, the mode volumes of the HG modes are smaller than those of the 3D coherent waves for low transverse orders. However, this situation becomes opposite when the transverse orders are sufficiently high. The 3D coherent waves consequently turn out to be a preferred set of resonant states in the high-order regime. For higher transverse orders, the macroscopic superposition states can lead to the total mode volumes being smaller. Therefore, it is possible to generate the macroscopic superposition states if the two superposed 3D coherent waves are simultaneously excited by controlling the pump distribution.

We recently used the off-axis pumping scheme to efficiently generate the 3D coherent waves localized on the Lissajous parametric surfaces in a symmetric laser cavity with extremely low losses [17]. However, the corresponding macroscopic superposition states were not manifestly observed because the clear aperture of the conventional gain medium was approximately 2 mm that was not large enough to generate the lasing modes with the transverse order greater than the critical number, as discussed in Fig. 4. To overcome this hindrance, we prepare a gain medium with a transverse aperture up to 8 mm in the present experiment. Figure 5 shows a photograph of the symmetric laser cavity. The spherical mirror was a 10-mm radius-of-curvature concave mirror with antireflection coating at the pumping wavelength on the entrance face ($R<0.2\%$), high-reflection coating at lasing wavelength ($R>99.8\%$), and high-transmission coating at the pumping wavelength on the other surface ($T>95\%$). The gain medium was a 2.0 at. % $Nd:YVO_4$ crystal with a longitudinal length of 2 mm and transverse cross section of 8×8 mm^2. Both surfaces of the laser crystal were coated for antireflection at the pumping and lasing wavelengths. The pump source was a 1-W 808-nm fiber-coupled laser diode with a core diameter of 100 μm and a numerical aperture of 0.16. A focusing lens was used to reimage the pump beam into the laser crystal. The pump radius was estimated to be 25 μm. A microscope objective lens mounted on a transla-

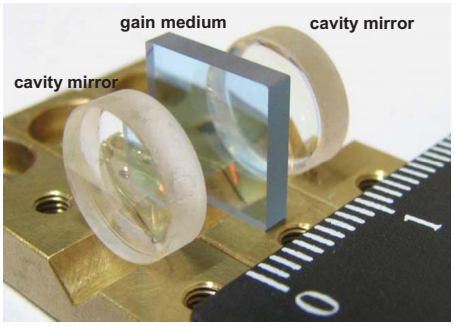

FIG. 5. (Color online) Photograph of the experimental laser cavity.

tion stage was used to reimage the tomographic transverse patterns inside the cavity onto a charge-coupled-device (CCD) camera.

With the off-axis pumping method, the transverse orders of the excited coherent waves can be up to the range of 100–1000. Experimental results reveal that numerous macroscopic superposition states can be stably generated by adjusting the cavity length in the range of 16–20 mm with a pump spot radius approximately 25 μm. The experimental far-field patterns were observed by directly projecting the output laser beam on a paper screen at a distance of ~50 cm from the laser cavity and were recorded by a digital camera. Figure 6 shows eight typical experimental far-field patterns observed in different cavity lengths. The experimental results depicted in the first and second rows of Fig. 6 are the macroscopic superposition states with dotted and dashed wave patterns localized on the Lissajous figures, respectively.

Figure 7 shows the experimental tomographic transverse patterns for $(p,q)=(3,-2)$ corresponding to $\Omega=1$. The tomographic transverse patterns inside the cavity can be clearly seen to display the revolution of the spatially localized patterns along the longitudinal axis to form a complete 3D interference pattern. More importantly, the experimental patterns are in good agreement with the feature of the theoretical results shown in Fig. 3. The structure of the spatially localized patterns is found to be highly stable. It is worthwhile to mention that the 3D coherent states have the properties of the pointer states which evolve into periodic

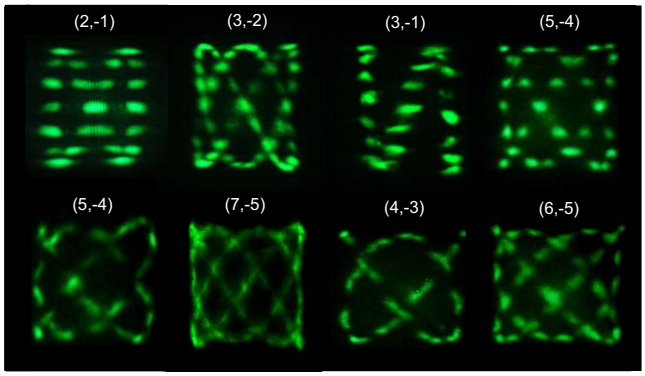

FIG. 6. (Color online) Typical experimental far-field patterns observed in different cavity lengths for different indices (p,q).

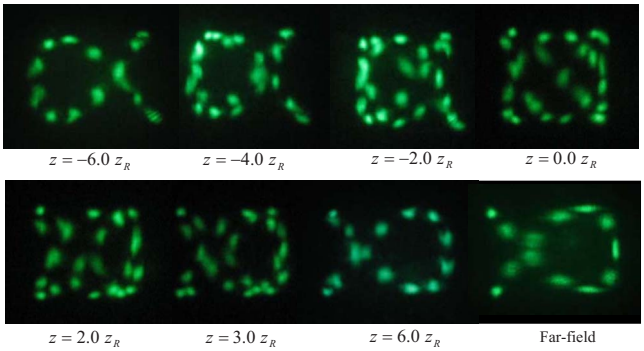

FIG. 7. (Color online) Experimental tomographic transverse patterns for $(p,q)=(3,-2)$ corresponding to $\Omega=1$.

rays and remain robust in the presence of the environment coupling [42–44]. To be explicit, the formation of 3D coherent waves is consistent with the process of the decoherence-induced selection of the preferred pointer states that was termed einselection [42,43].

Further increasing the pump-to-mode size ratio, the superhigh-order coherent modes can be generated flexibly and superposition of the coherent modes can be achieved in the laser cavity. Figure 8 shows the dotlike interference patterns of the superposition of the superhigh-order coherent modes with strong localization on Lissajous figures. The indices (p,q) are generally limited by the magnitude of the excited transverse orders.

IV. CONCLUSION

The 3D coherent laser modes that form a preferred set in high-order degenerate cavities have been employed to investigate the spatial features of macroscopic superposition states in an analogous way. Numerical analysis reveals that the spatial beating leads to the characteristic morphology of macroscopic superposition states to be dashed and dotted wave patterns, the distinction of which is dependent on the difference between the transverse orders of two 3D coherent states. Moreover, we have calculated the mode volumes of various stationary high-order modes to explore the prospect of generating macroscopic superposition states. Finally, we have used a large-aperture laser system to experimentally realize the macroscopic superposition states. The structures

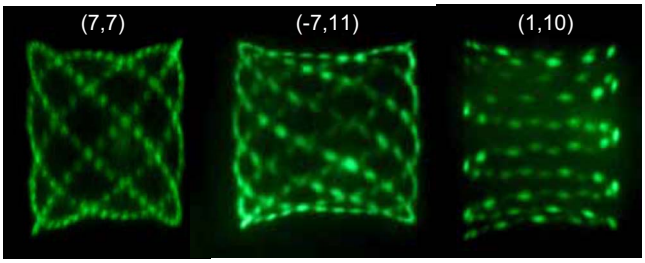

FIG. 8. (Color online) Experimental far-field patterns for the macroscopic superposition of the superhigh-order coherent modes.

of the macroscopic superposition states are also experimentally confirmed to be highly stable and easily reproducible. The essential properties of the cavity for observing the macroscopic superposition states are mainly composed of the longitudinal-transverse coupling, the mode-locking effect, and the larger aperture for generation of high-order transverse modes. The present results certainly proffer informative insights into the spatial morphology of the coherent superposition in mesoscopic and macroscopic regimes.

[1] G. S. Agarwal and P. K. Pathak, Phys. Rev. A **70**, 053813 (2004).
[2] E. G. Cavalcanti and M. D. Reid, Phys. Rev. Lett. **97**, 170405 (2006).
[3] S. B. Zheng, Phys. Rev. A **75**, 032114 (2007).
[4] E. Schrödinger, Naturwiss. **23**, 807 (1935); , **23**, 823 (1935); , **23**, 844 (1935).
[5] M. W. Noel and C. R. Stroud, Jr., Phys. Rev. Lett. **77**, 1913 (1996).
[6] M. Brune, E. Hagley, J. Dreyer, X. Maitre, A. Maali, C. Wunderlich, J. M. Raimond, and S. Haroche, Phys. Rev. Lett. **77**, 4887 (1996).
[7] J. R. Friedman, V. Patel, W. Chen, S. K. Tolpygo, and J. E. Lukens, Nature (London) **406**, 43 (2000).
[8] *Quantumlike Models and Coherent Effects*, edited by R. Fedele and P. K. Shukla (World Scientific, Singapore, 1995).
[9] V. I. Karpmann, *Nonlinear Waves in Dispersive Media* (Pergamon Press, Oxford, 1975).
[10] G. P. Agrawal, *Nonlinear Fiber Optics* (Academic Press, San Diego, 1995).
[11] *New Perspectives in Physics of Mesoscopic Systems: Quantumlike Descriptions and Macroscopical Coherent Phenomena*, edited by S. De Martino, S. De Nicola, S. De Siena, R. Fedele, and G. Miele (World Scientific, Singapore, 1995).
[12] G. Nienhuis and L. Allen, Phys. Rev. A **48**, 656 (1993).
[13] C. Gmachl, F. Capasso, E. E. Narimanov, J. U. Nöckel, A. D. Stone, J. Faist, D. L. Sivco, and A. Y. Cho, Science **280**, 1556 (1998).
[14] N. B. Rex, H. E. Tureci, H. G. L. Schwefel, R. K. Chang, and A. D. Stone, Phys. Rev. Lett. **88**, 094102 (2002).
[15] M. Lebental, J. S. Lauret, J. Zyss, C. Schmit, and E. Bogomolny, Phys. Rev. A **75**, 033806 (2007).
[16] A. E. Kaplan, I. Marzoli, W. E. Lamb, Jr., and W. P. Schleich, Phys. Rev. A **61**, 032101 (2000).
[17] K. F. Huang, Y. F. Chen, H. C. Lai, and Y. P. Lan, Phys. Rev. Lett. **89**, 224102 (2002).
[18] T. Gensty, K. Becker, I. Fischer, W. Elsäßer, C. Degen, P. Debernardi, and G. P. Bava, Phys. Rev. Lett. **94**, 233901 (2005).
[19] Y. F. Chen, K. W. Su, T. H. Lu, and K. F. Huang, Phys. Rev. Lett. **96**, 033905 (2006).
[20] E. J. Galvez, P. R. Crawford, H. I. Sztul, M. J. Pysher, P. J. Haglin, and R. E. Williams, Phys. Rev. Lett. **90**, 203901 (2003).
[21] I. Vorobeichik, E. Narevicius, G. Rosenblum, M. Orenstein, and N. Moiseyev, Phys. Rev. Lett. **90**, 176806 (2003).
[22] M. Brambilla, F. Battipede, L. A. Lugiato, V. Penna, F. Prati, C. Tamm, and C. O. Weiss, Phys. Rev. A **43**, 5090 (1991).
[23] D. Dangoisse, D. Hennequin, C. Lepers, E. Louvergneaux, and P. Glorieux, Phys. Rev. A **46**, 5955 (1992).
[24] E. Louvergneaux, D. Hennequin, D. Dangoisse, and P. Glorieux, Phys. Rev. A **53**, 4435 (1996).
[25] E. Louvergneaux, G. Slekys, D. Dangoisse, and P. Glorieux, Phys. Rev. A **57**, 4899 (1998).
[26] S. P. Hegarty, G. Huyet, J. G. McInerney, and K. D. Choquette, Phys. Rev. Lett. **82**, 1434 (1999).
[27] Y. F. Chen and Y. P. Lan, Phys. Rev. A **65**, 013802 (2001).
[28] F. Encinas-Sanz, S. Melle, and O. G. Calderón, Phys. Rev. Lett. **93**, 213904 (2004).
[29] E. Cabrera, O. G. Calderón, S. Melle, and J. M. Guerra, Phys. Rev. A **73**, 053820 (2006).
[30] G. P. Karman, G. S. McDonald, G. H. C. New, and J. P. Woerdman, Nature (London) **402**, 138 (1999).
[31] Y. F. Chen, Y. P. Lan, and K. F. Huang, Phys. Rev. A **68**, 043803 (2003).
[32] Y. F. Chen and K. F. Huang, J. Phys. A **36**, 7751 (2003).
[33] A. J. Makowski, J. Phys. A **38**, 2299 (2005).
[34] Y. F. Chen, T. H. Lu, K. W. Su, and K. F. Huang, Phys. Rev. E **72**, 056210 (2005).
[35] K. J. Górska, A. J. Makowski, and S. T. Dembiński, J. Phys. A **39**, 13285 (2006).
[36] Y. F. Chen, T. H. Lu, K. W. Su, and K. F. Huang, Phys. Rev. Lett. **96**, 213902 (2006).
[37] A. E. Siegman, *Lasers* (University Science Books, Mill Valley, CA, 1986).
[38] L. A. Openov, Solid State Commun. **113**, 549 (2005).
[39] Y. Y. Schechner, R. Piestun, and J. Shamir, Phys. Rev. E **54**, R50 (1996).
[40] Y. Hlushchuk and S. Russ, Phys. Rev. E **68**, 016203 (2003).
[41] F. Wegner, Z. Phys. B **36**, 209 (1980).
[42] J. P. Paz and W. H. Zurek, Phys. Rev. Lett. **82**, 5181 (1999).
[43] D. K. Ferry, R. Akis, and J. P. Bird, Phys. Rev. Lett. **93**, 026803 (2004).
[44] J. Wiersig, Phys. Rev. Lett. **97**, 253901 (2006).